Achievement of a Giant Electromechanical Conversion Coefficient in a Molecular-based Ferroelectric

Bin Wang †, Zhirui Li †, Zhengxiao Tang, Haixia Zhao *, Lasheng Long *, Lansun Zheng

Collaborative Innovation Center of Chemistry for Energy Materials, State Key Laboratory of Physical Chemistry of Solid Surfaces and Department of Chemistry, College of Chemistry and Chemical Engineering, Xiamen University, Xiamen, 361005, Fujian. China.

*Correspondence: hxzhao@xmu.edu.cn; lslong@xmu.edu.cn

1. Experiment section

XRD measurement

X-ray crystallographic and powder X-ray diffraction (PXRD) measurements. The single crystal data for **1** were collected using an Agilent Supernova CCD diffractometer utilizing Cu K_α radiation (λ = 1.54178 Å) in ω-scan mode ($\Delta\omega$ = 1.0°) at room temperature. The CrysAlis PRO program was applied to execute data collection, cell refinement and data reduction. The structures were determined by direct methods using ShelXT and refined by full-matrix least squares on F^2 by using ShelXL in the OLEX2 program. CCDC 2190250 (**1**) can be obtained free of charge from the Cambridge Crystallographic Data Centre and contain the supplementary crystallographic data for this paper.

TG measurement

Thermogravimetric analyses (TG) were performed with alumina crucibles by using an SDT-Q600 thermal analyzer (TA instrument) operated at a heating rate of 10 K·min^{-1} under an air atmosphere.

SHG measurement

Optical second harmonic generation (SHG) measurements were carried out with an integrated instrument, which ensured low divergence (pulsed Nd:YAG at a wavelength of 1064 nm, 10 Hz repetition rate, 1.6 MW peak power, 5 ns pulse duration) for the unexpanded laser (OPOTEK, 355 II). SHG experiments were performed using powder samples at room temperature.

***d_{33}* measurement**

The powder samples underwent a 12-hour drying process in a vacuum drying oven. Polycrystalline pellets were fabricated through a prototype-mold with a diameter of 10 mm under a pressure of approximately 20 MPa. And the thickness is around 0.5 mm. Electrodes were formed by applying silver paste to both sides of the films. The prepared sample with electrodes were subjected to 30 kV/cm electric field on high-voltage polarization device (DW-P303-1ACDF0, DONG WEN VOLTAGE, China) for a duration of for 30 mins at room temperature. Then, calibrate the d_{33} measuring instrument (ZJ-6A). After that, both electrode-painted surfaces of polycrystalline pellet of **1** were connected to the two probes of the d_{33} meter. Measure at least 10 samples following the standard sample test procedure in order to ensure the reliability of test results. And the d_{33} of polycrystalline pellet of **1** was measured in forward and reverse connection.

***S–E* curves measurement**

The strain versus electric field (*S*–*E*) curves were measured in a silicon oil bath by applying an electric field with a triangular waveform at 25 Hz by employing a ferroelectric testing system (Radiant Precision Premier II Technology) coupled with an MTI 2100 photonic sensor.

Dielectric constant measurement

Dielectric constant measurements were carried out on a Wayne Kerr 6500B analyzer. The dielectric permittivity ε $(\varepsilon = \varepsilon' - i\varepsilon'')$ measurements adopted the two-probe *a.c.* impedance method. For dielectric constant measurements, sample pellets were prepared with an area and thickness of 78 mm^2 and 0.15 mm, respectively**.**

***P-E* curves measurement:**

A Radiant Precision Premier II analyzer was used in the polarization−electric field (*P*-*E*) hysteresis loop measurements. Small electric conductivity contributions were eliminated by adopting the positive up negative down (PUND) method. The polycrystalline thin films were fabricated by slowly evaporating a drop of aqueous solution of **1** onto freshly cleaned ITO-coated glass. The *P*-*E* hysteresis loop measurements were conducted with the copper electrode/sample film/ITO architecture.

2. Supplementary Figures

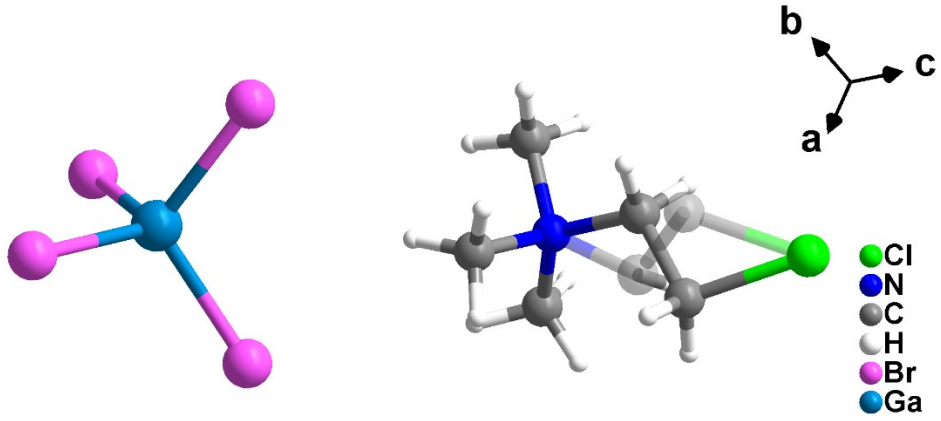

Fig. S1 The asymmetric unit of **1** at room temperature.

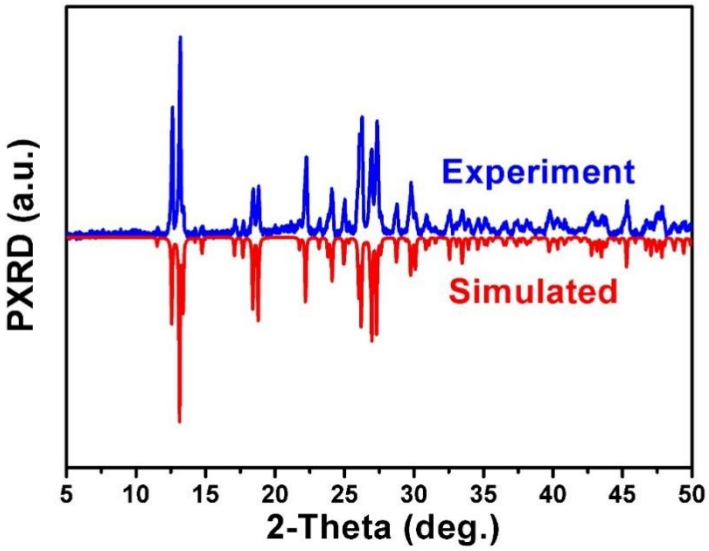

Fig. S2 PXRD data of **1** at room temperature.

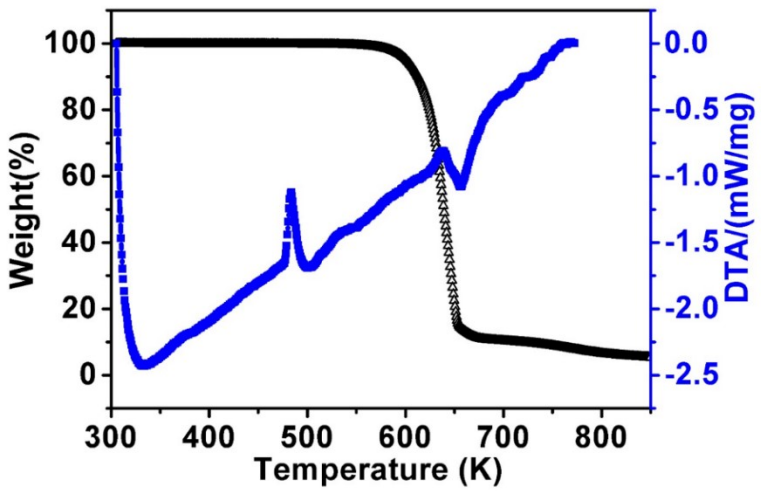

Fig. S3 TG data for **1**.

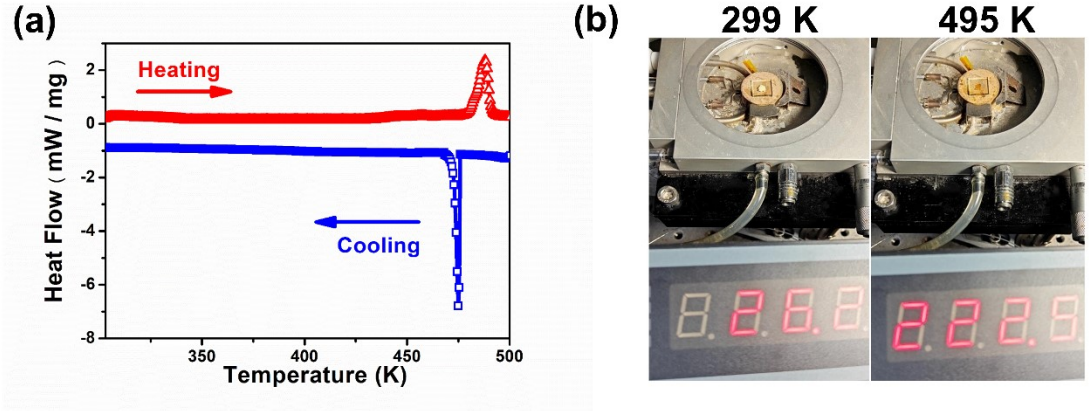

Fig. S4 (a) DSC curves; (b) the photo of compound **1** melting.

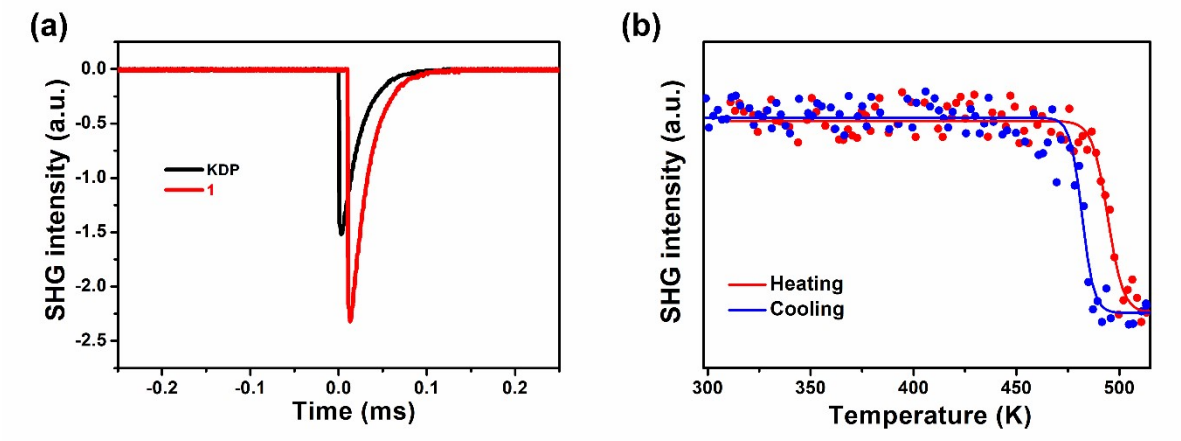

Fig. S5 SHG data for **1**. (a) the SHG response at room temperature; (b) the temperature dependent SHG response.

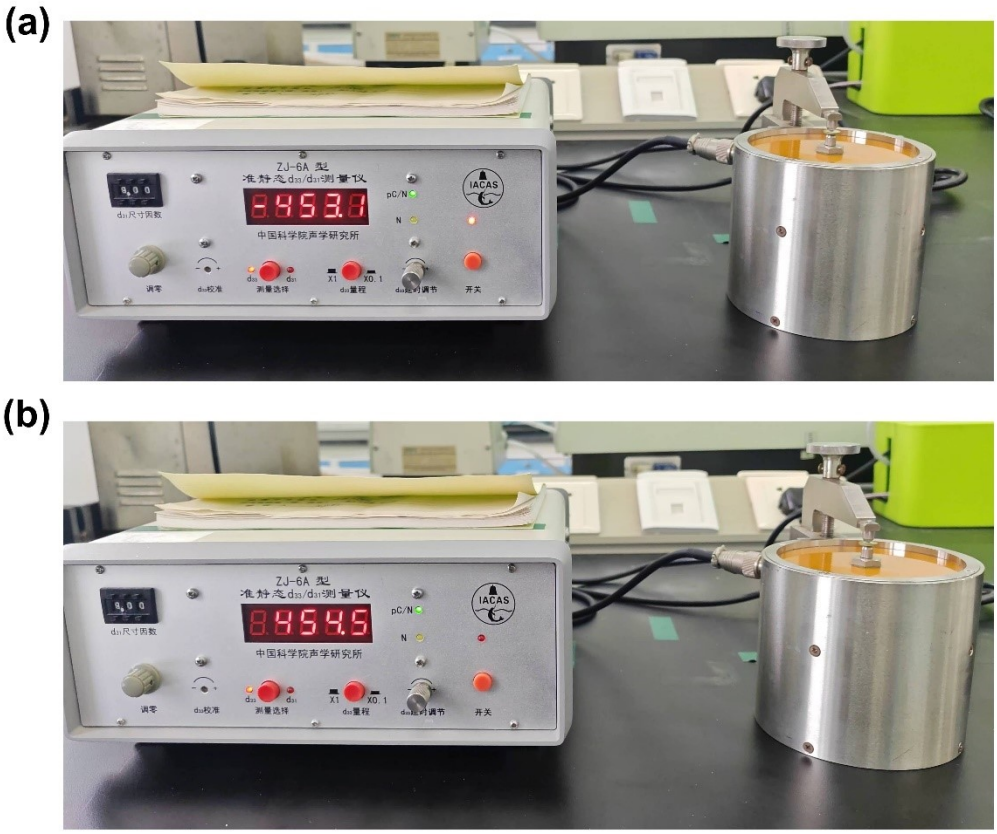

Fig. S6 Piezoelectric d_{33} data of polycrystalline pellet of **1** in reverse (a) and forward (b) connection.

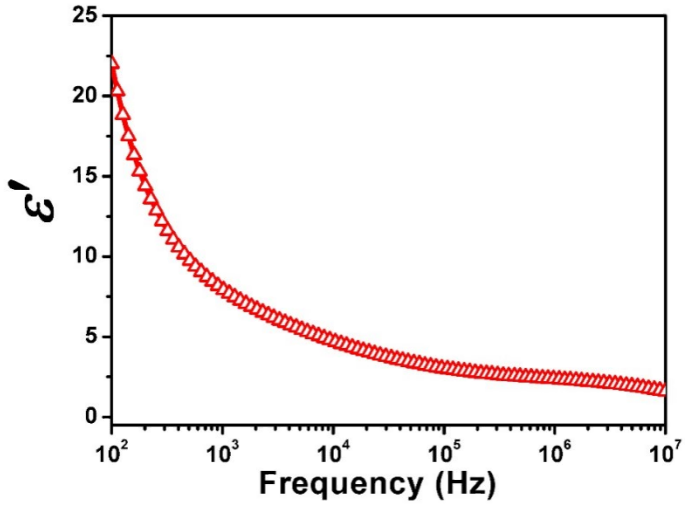

Fig. S7 Frequency dependence of ε' for **1** measured at room temperature with powder samples.

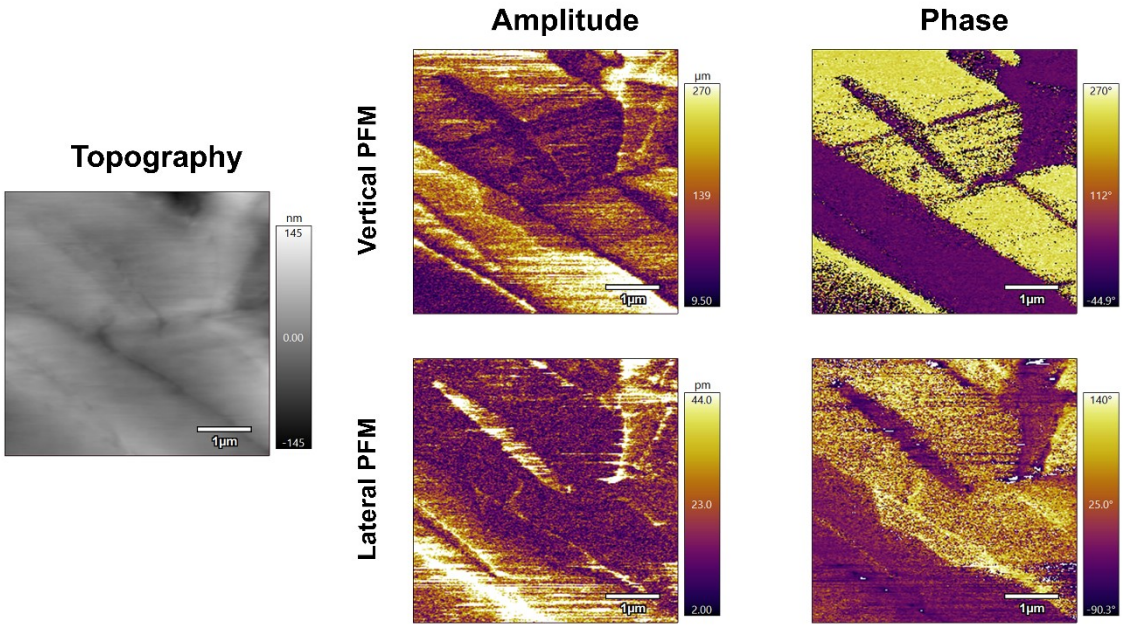

Fig. S8 Another set of PFM images including topography image; vertical and lateral PFM amplitudes and phase images.

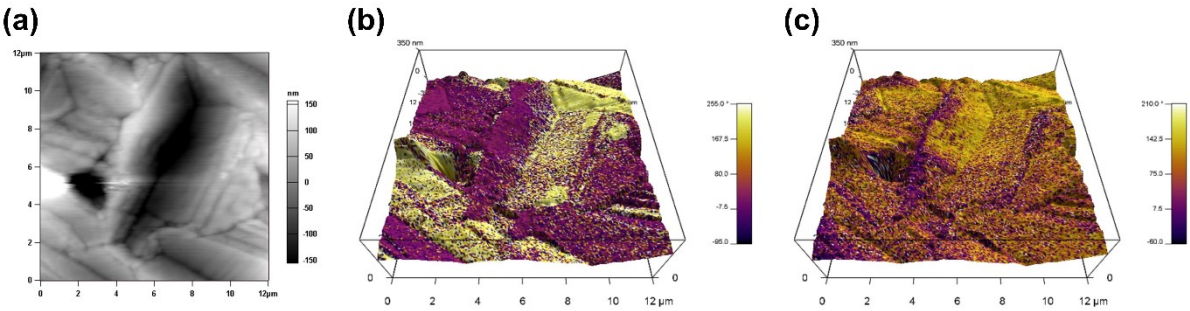

Fig. S9 Topography images of PFM. (a) Topography images; lateral (b) and vertical (c) PFM phase images overlaid on the 3D topography of the surface for a thin film of **1**.

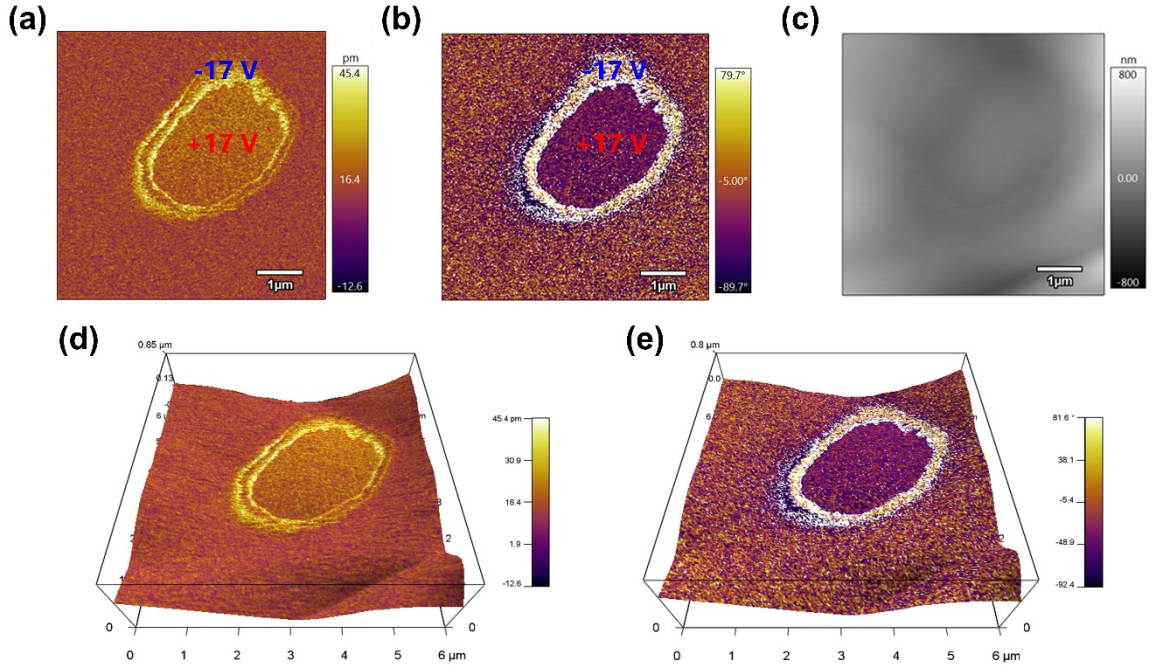

Fig. S10 The reversible polarization switching by the electric field. (a) PFM amplitudes, (b) phase and (c) topography images; (d) PFM amplitudes images and (e) phase images overlaid on the 3D topography.

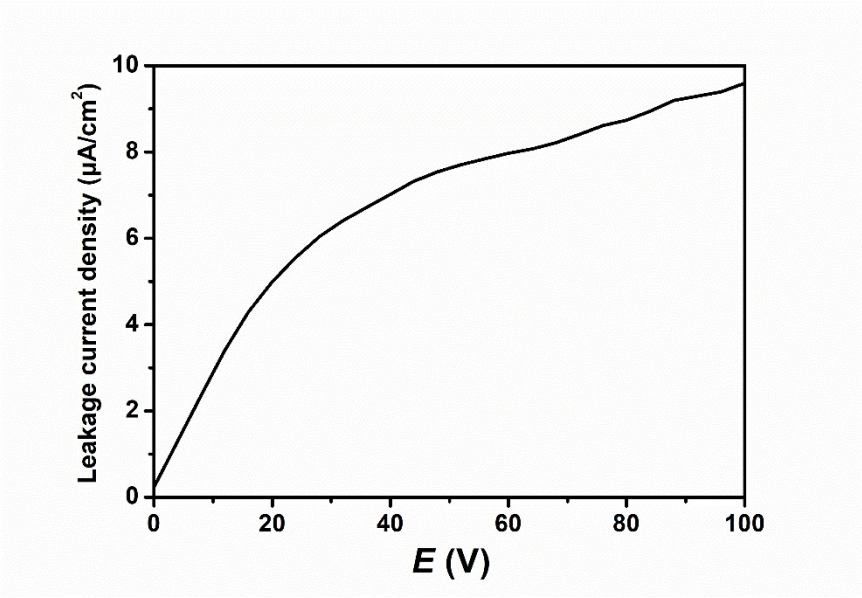

Fig. S11 The leakage current density of compound **1**.

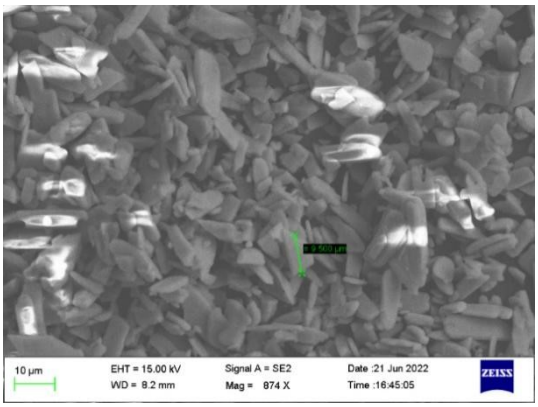

Fig. S12 SEM image for particles of **1**.

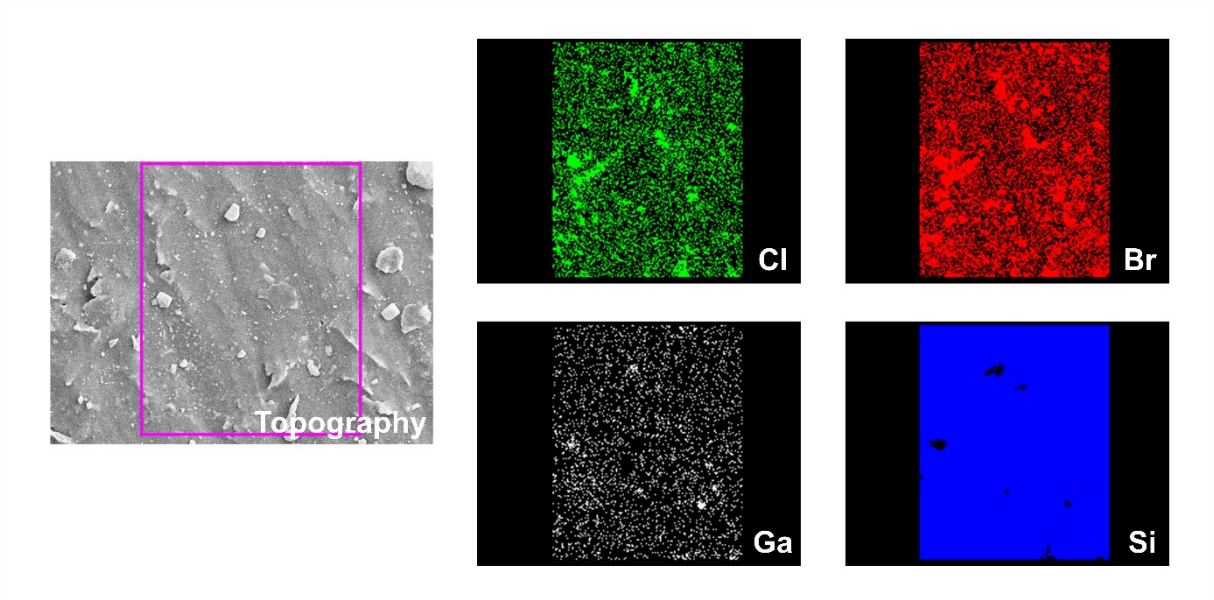

Fig. S13 Scanning electron microscopy (SEM) and mapping images for the 15 wt% **1**@PDMS film surface.

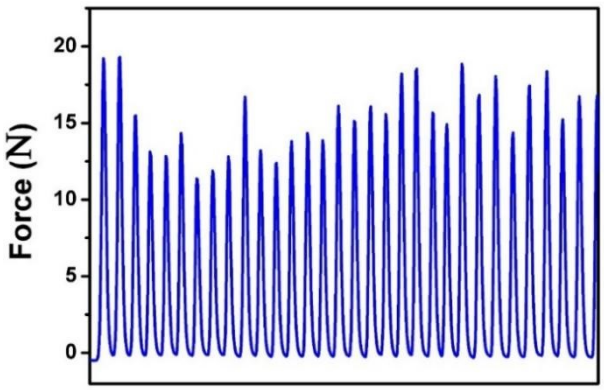

Fig. S14 Plots of force applied with thumb pressure.

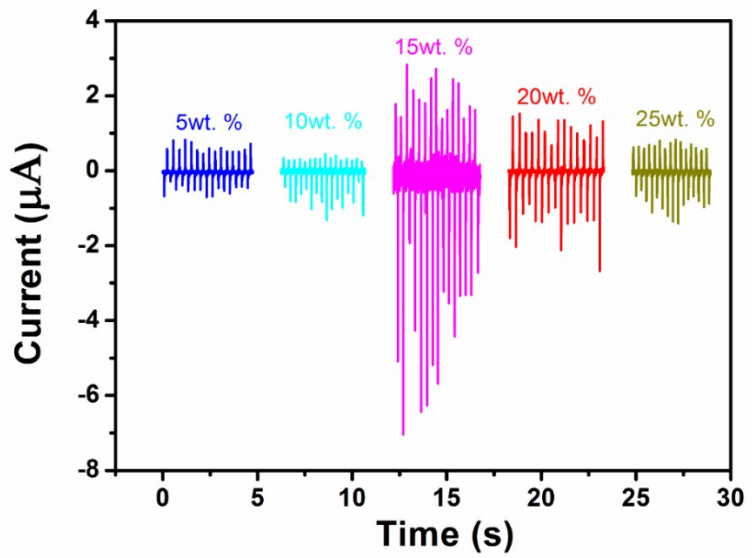

Fig. S15 I_{sc} data for **1**@PDMS with different mass fractions with thumb pressure.

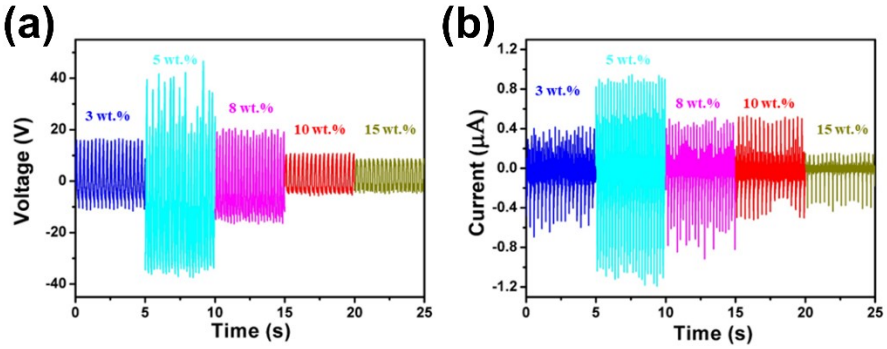

Fig. S16 The performance of **1**@PDMS built by sample after grinding with different mass fractions. (a) V_{oc} data; (b) I_{sc} data.

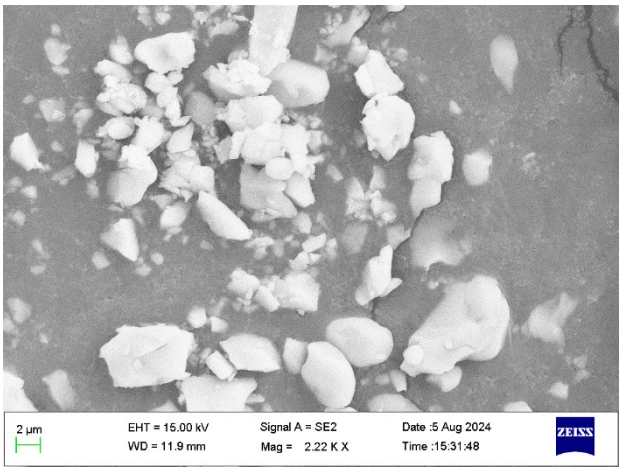

Fig. S17 SEM image of the ground sample **1**. The ground sample particles do not exhibit any specific morphology and exhibit irregular sizes, with the presence of large agglomerated particles (> 5 µm).

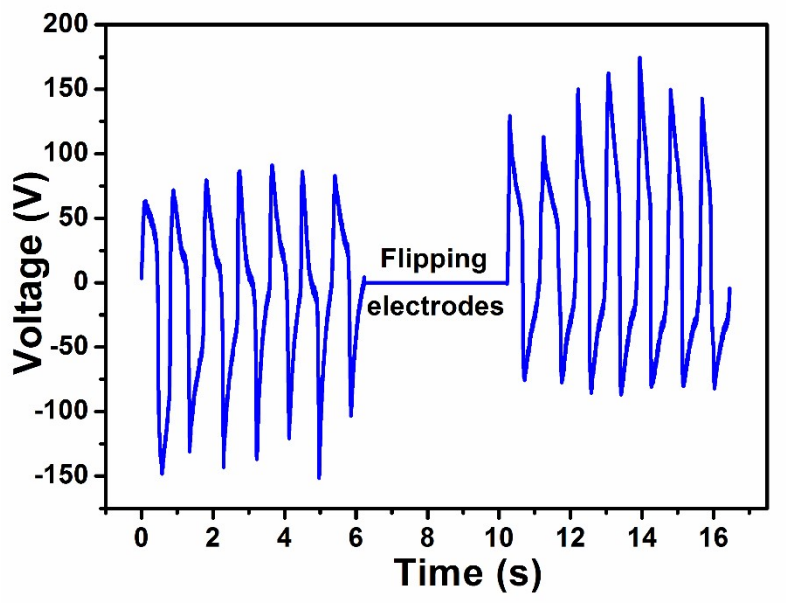

Fig. S18 V_{oc} for 15 wt% **1**@PDMS PEGs when flipping the electrodes.

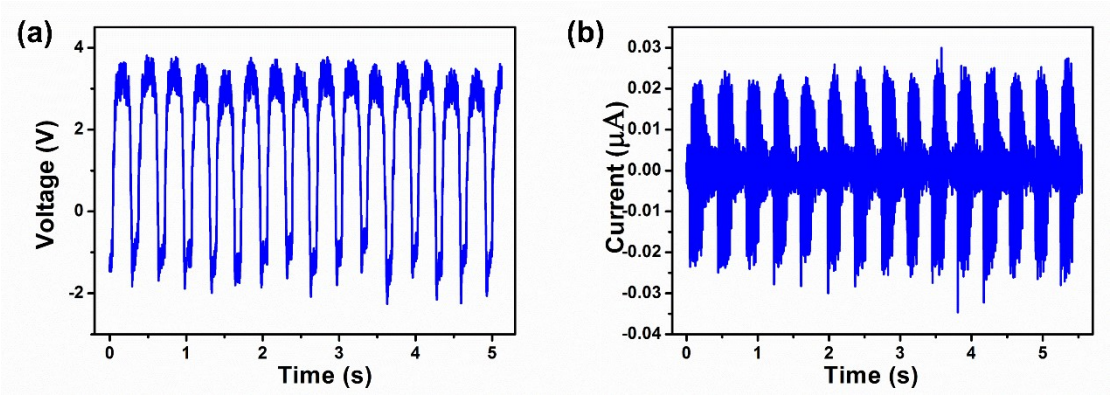

Fig. S19 The performance of pure PDMS with thumb pressure. (a) V_{oc} data; (b) I_{sc} data.

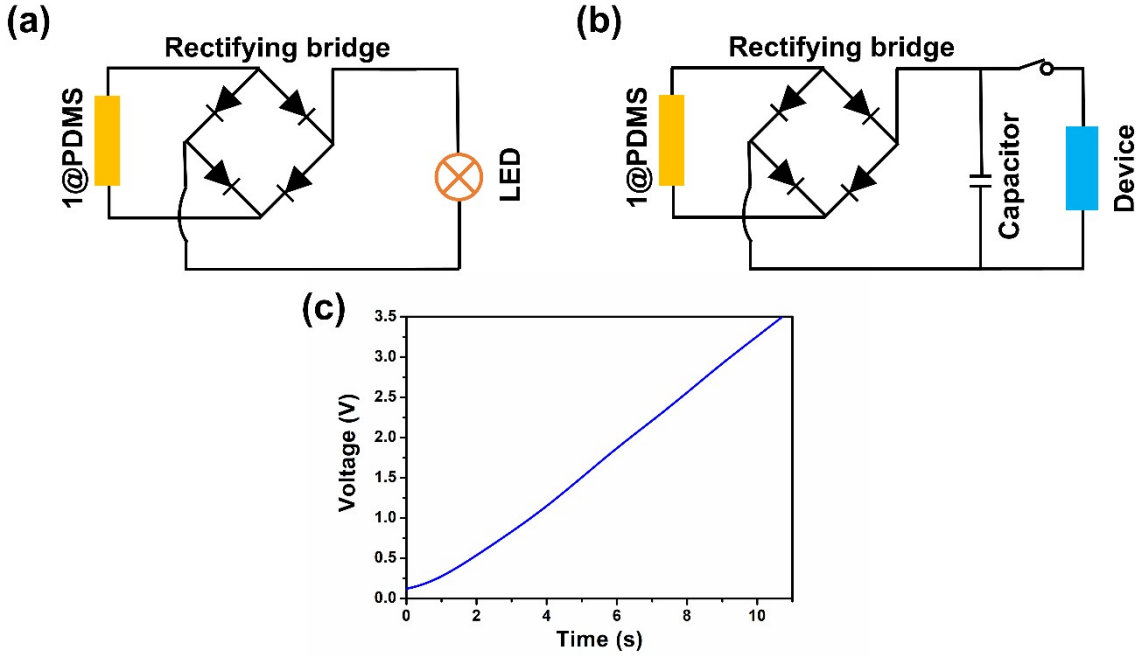

Fig. S20 Charge transfer circuit. (a) 15% **1**@PDMS with a full-wave rectifying bridge to power 100 LEDs; (b) 15% **1**@PDMS with a full-wave rectifying bridge and a 3.3 μF parallel capacitor to power a calculator / an electronic watch; (c) voltage-charging time of charging 3.3 μF capacitors using 15% **1**@PDMS.

3. Supplementary Tables

Table S1 Crystal data for **1** at 300 K.

Compound	**1**
Empirical formula	$C_5H_{13}Br_4ClGaN$
Formula weight	514.19
Temperature (K)	293(2)
Crystal system	orthorhombic
Space group	$Pca2_1$
a (Å)	14.0655(8)
b (Å)	7.6705(5)
c (Å)	13.2164(7)
α (deg.)	90
β (deg.)	90
γ (deg.)	90
V (Å^3)	1425.91(14)
Z	4
ρ_{cal} (g · cm^{-3})	2.395
μ (mm^{-1})	17.295
F(000)	956.0
Reflections collected	3153
R_{int}	0.0408
Data/restraints/parameters	1616/102/132
GOOFs	1.055
R_1/wR_2 $[I > 2\sigma(I)]$	R_1 = 0.0616, wR_2 = 0.1595
R_1/wR_2 *(all data)*	R_1 = 0.0761, wR_2 = 0.1809
Largest diff. peak/hole (e · Å^{-3})	1.12/-1.18

Table S2 Distances between the Br atoms of the $[GaBr_4]^-$ anion and surrounding atoms.

	bond lengths [Å]		bond lengths [Å]
Br1—C5^{i}	3.528	Br1—C2^{ii}	3.890
Br1—Br4^{iii}	3.880	Br2—C7	3.889
Br2—C5A	3.737	Br2—C5^{iv}	3.708
Br2—C2^{v}	3.880	Br3—C5A^{vi}	3.554
Br3—Br4^{vii}	3.915		

Symmetry codes: (i) 2-x, 2-y, 1/2+z; (ii) 2-x, 3-y, 1/2+z; (iii) x+1/2, 3-y, z; (iv) x+1/2, 2-y, -z; (v) x-1/2, 3-y, z; (vi) -x+3/2, y, z+1/2; (vii) x, y-1, z.

Table S3 The g_{33} and d_{33} values of **1** and other molecular ferroelectrics.

samples	d_{33} (pC·N^{-1})	g_{33} (× 10^{-3} V·m·N^{-1})	Crystal form	Reference
DIPAB	11	19.7	Single crystal	1
TGS	22	37	Single crystal	1
Croconic acid (CA)	5	47.1	Single crystal	1
Imidazolium perchlorate	41	257.3	Single crystal	2
$(ATHP)_2PbBr_4$	75	660	Single crystal	3
$TMCM_2SnCl_6$	137	980	Single crystal	4
$TMCMMnCl_3$	185	1681	Single crystal	1
$TMBMMnBr_3$	112	1120	Single crystal	5
$TMCMCdBr_3$	139	1962	Single crystal	6
MDABCO-NH_4I_3	14	79	Single crystal	7
$C_6H_5N(CH_3)_3CdBr_2Cl_{0.75}I_{0.25}$	324	3595	Single crystal	8
$(TMFM)_x(TMCM)_{1-x}CdCl_3$	1540	9506	Single crystal	9
NDABCO-NH_4-Br_3	63	252	Single crystal	10
$[Me_3NCH_2Cl]CdBrCl_2$	440	6215	Single crystal	11
$(HaaOH)BF_4$	22	165.7	Single crystal	12
$[Ph_3MeP]_4[Ni(NCS)_6]$	8	63.27	Single crystal	13
[3.2.1-abco]ReO_4	118	131	polycrystalline	14
NMe_3BH_3	10–16	174-278	polycrystalline	15
$[C(NH_2)_3][ClO_4]$	15	292	polycrystalline	16
$[(CH_3)_4N][FeCl_4]$	80	1434	polycrystalline	17
$[(CH_3)_4N][FeBrCl_3]$	110	1420	polycrystalline	17
$[(CH_3)_4N][GaCl_4]$	80	2008	polycrystalline	18
[AH][ReO4]	90	338	polycrystalline	19
$TMCMGaCl_4$	226	1318	polycrystalline	20
1	454	10910	polycrystalline	This work

Table S4 The $d_{33}\times g_{33}$ of **1** vs. other ferroelectrics.

Sample	d_{33} (pC·N^{-1})	g_{33} (× 10^{-3} V·m·N^{-1})	$d_{33}\times g_{33}$ (× 10^{-12} m^2·N^{-1})	Reference
PZT507	700	20.0	14	21
APC855	620	21.0	12.6	21
Pz39	480	30.0	14.4	21
PIN-PMN-PT	3480 (d_{15})	37.25 (g_{15})	129.6	22
Soft ceramic	920 (d_{15})	38.72 (g_{15})	35.9	22
PVDF	33	286.7	9.46	23
$(ATHP)_2PbBr_4$	75	660.3	50.2	3
$TMCM_2SnCl_6$	137	980	134.3	4
$TMCMMnCl_3$	185	1681	311	1
$TMCMCdBr_3$	139	1962	272.7	6
$C_6H_5N(CH_3)_3CdBr_2Cl_{0.75}I_{0.25}$	324	3595	1222.8	8
$[N(CH_3)_4]FeCl_4$	80	1434	114.7	17
$[N(CH_3)_4]GaCl_4$	80	2008	160.6	18
$[N(CH_3)_3CH_2Cl]GaCl_4$	226	5672	1281.9	20
1	454	10910	4953.1	This work

Table S5 The P_s, d_{33} and g_{33} values of **1** and other similar molecular ferroelectrics.

Sample	P_s (μC·cm^{-2})	d_{33} (pC·N^{-1})	g_{33} (× 10^{-3} V·m·N^{-1})	Reference
$[N(CH_3)_4]FeCl_4$	2.0	80	1434	17
$[N(CH_3)_4]GaCl_4$	3.8	80	2008	18
$[N(CH_3)_3CH_2Cl]GaCl_4$	6.4	226	5672	20
1	9.5	454	10910	This work

Table S6 The dipole moment values of organic cations.

Organic cations	*Dipole moment (Debye)
$[N(CH_3)_4]^+$	0
$[N(CH_3)_3CH_2Cl]^+$	4.24
$[N(CH_3)_3CH_2CH_2Cl]^+$	6.73

Note: *Dipole moment value was determined theoretically by utilizing Gaussian 09 software at the B3LYP/def2TZVP level of theory.

Table S7 Power density of **1**@PDMS vs. those for PEGs previously used in the same PDMS matrix.

Piezoelectric Materials	Pressure	V_{oc} (V)	J_{sc} ($\mu A \cdot cm^{-2}$)	Power density ($\mu W \cdot cm^{-2}$)	ref
$[Me_3NCH_2CH_2OH]CdCl_3$−PDMS	40 N	55.2	4.02	70.9	24
$[(ATHP)_2PbBr_2Cl_2$@PDMS]	4.2 N	90	6.5 μA	1.7	25
$[BnNMe_3]CdBr_4$/PDMS	40 N	52.9	0.23	13.8	26
$[BnNMe_2{}^nPr]_2CdBr_4$/PDMS	40 N	63.8	0.59	37.1	26
$MAPbI_3$-PDMS	-	100	0.27	30	27
$(BTMA)_2CoBr_4$/PDMS	2.5 N	19.7	2.94	11.72	28
$MASnBr_3$−PDMS	0.5 MPa	18.8	13.76	74.52	29
$[(CH_3)_3NCH_2Cl][GaCl_4]$@PDMS	1 N	38.1	1.6	-	20
DPDP·PF_6/PDMS	15 N	8.5	0.28	0.13	30
$TMCM_2SnCl_6$@PDMS	4.9 N	81	2 μA	2.56	4
$FAPbBr_3$–PDMS	0.5 MPa	8.5	3.4	12	31
1@PDMS	20 N	179	1.6	120	This work

-: Pressure and power density values were not provided for reported ferroelectrics.

References

(1) Y. M. You, W. Q. Liao, D. W. Zhao, H. Y. Ye, Y. Zhang, Q. H. Zhou, X. H. Niu, J. L. Wang, P. F. Li, D. W. Fu, Z. M. Wang, S. Gao, K. L. Yang, J. M. Liu, J. Y. Li, Y. F. Yan, R. G. Xiong, An organic-inorganic perovskite ferroelectric with large piezoelectric response, Science 357 (2017) 306-309.

(2) Y. Zhang, Y. M. Liu, H. Y. Ye, D. W. Fu, W. X. Gao, H. Ma, Z. G. Liu, Y. Y. Liu, W. Zhang, J. Y. Li, G. L. Yuan, R. G. Xiong, A molecular ferroelectric thin film of imidazolium perchlorate that shows superior electromechanical coupling, Angew. Chem., Int. Ed. 53 (2014) 5064-5068.

(3) X. G. Chen, X. J. Song, Z. X. Zhang, P. F. Li, J. Z. Ge, Y. Y. Tang, J. X. Gao, W. Y. Zhang, D. W. Fu, Y. M. You, R. G. Xiong, Two-Dimensional Layered Perovskite Ferroelectric with Giant Piezoelectric Voltage Coefficient, J. Am. Chem. Soc. 142 (2020) 1077-1082.

(4) G. G. Huang, A. A. Khan, M. M. Rana, C. Xu, R. Saritas, S. Zhang, E. Abdel-Rahmand, P. Turban, S. Ababou-Girard, C. L. Wang, D. Y. Ban, Achieving Ultrahigh Piezoelectricity in Organic−Inorganic Vacancy-Ordered Halide Double Perovskites for Mechanical Energy Harvesting, ACS Energy Lett. 6 (2021) 16-23.

(5) W. Q. Liao, Y. Y. Tang, P. F. Li, Y. M. You, R. G. Xiong, Large Piezoelectric Effect in a Lead-Free Molecular Ferroelectric Thin Film, J. Am. Chem. Soc. 139 (2017) 18071−18077.

(6) W. Q. Liao, Y. Y. Tang, P. F. Li, Y. M. You, R. G. Xiong, Competitive Halogen Bond in the Molecular Ferroelectric with Large Piezoelectric Response, J. Am. Chem. Soc. 140 (2018) 3975-3980.

(7) H. Y. Ye, Y. Y. Tang, P. F. Li, W. Q. Liao, J. X. Gao, X. N. Hua, H. Cai, P. P. Shi, Y. M. You, R. G. Xiong Metal-free three-dimensional perovskite ferroelectrics, Science 361 (2018) 151–155.

(8) Y. Z. Hu, K. Parida, H. Zhang, X. Wang, Y. X. Li, X. R. Zhou, S. A. Morris, W. H. Liew, H. M. Wang, T. Li, F. Jiang, M. M. Yang, M. Alexe, Z. H. Du, C. L. Gan, K. Yao, B. Xu, P. S. Lee, H. J. Fanet, Bond engineering of molecular ferroelectrics renders soft and high-performance piezoelectric energy harvesting materials, Nat. Commun. 13 (2022) 5607.

(9) W. Q. Liao, D. W. Zhao, Y. Y. Tang, Y. Zhang, P. F. Li, P. P. Shi, X. G. Chen, Y. M. You, R. G. Xiong, A molecular perovskite solid solution with piezoelectricity stronger than lead zirconate titanate, Science 363 (2019) 1206-1210.

(10) H. Zhang, Z. K. Xu, Z. X. Wang, H. Yu, H. P. Lv, P. F. Li, W. Q. Liao, R. G. Xiong, Large Piezoelectric Response in a Metal-Free Three-Dimensional Perovskite Ferroelectric, J. Am. Chem. Soc. 145 (2023) 4892−4899.

(11) X. G. Chen, Y. Y. Tang, H. P. Lv, X. J. Song, H. Peng, H. Yu, W. Q. Liao, Y. M. You, R. G. Xiong, Remarkable Enhancement of Piezoelectric Performance by Heavy Halogen Substitution in Hybrid Perovskite Ferroelectrics, J. Am. Chem. Soc. 145 (2023) 1936−1944.
(12) Y. A. Xiong, S. S. Duan, H. H. Hu, J. Yao, Q. Pan, T. T. Sha, X. Wei, H. R. Ji, J. Wu, Y. M. You, Enhancement of phase transition temperature through hydrogen bond modification in molecular ferroelectrics, Nat. Commun. 15 (2024) 4470.
(13) T. Vijayakanth, F. Ram, B. Praveenkumar, K. Shanmuganathan, R. Boomishankar. Piezoelectric Energy Harvesting from a Ferroelectric Hybrid Salt $[Ph_3MeP]_4[Ni(NCS)_6]$ Embedded in a Polymer Matrix, Angew. Chem. Int. Ed. 59 (2020) 10368–10373.
(14) Y. Ai, P. F. Li, X. G. Chen, H. P. Lv, Y. R. Weng, Y. Shi, F. Zhou, R. G. Xiong, W. Q. Liao, The First Ring Enlargement Induced Large Piezoelectric Response in a Polycrystalline Molecular Ferroelectric, Adv. Sci. 10 (2023) 2302426.
(15) Y. Zhang, A. M. Hopkins, D. J. Liptrot, H. Khanbareh, P. Groen, X. F. Zhou, D. Zhang, Y. X. Bao, K. C. Zhou, C. R. Bowen, D. R. Carbery, Harnessing Plasticity in an Amine-Borane as a Piezoelectric and Pyroelectric Flexible Film, Angew. Chem. Int. Ed. 59 (2020) 7808-7812.
(16) Q. Pan, Z. B. Liu, H. Y. Zhang, W. Y. Zhang, Y. Y. Tang, Y. M. You, P. F. Li, W. Q. Liao, P. P. Shi, R. W. Ma, R. Y. Wei, R. G. Xiong, A Molecular Polycrystalline Ferroelectric with Record-High Phase Transition Temperature, Adv. Mater. 29 (2017) 1700831-1700837.
(17) D. Li, X. M. Zhao, H. X. Zhao, X. W. Dong, L. S. Long, L. S. Zheng, Construction of Magnetoelectric Composites with a Large Room-Temperature Magnetoelectric Response through Molecular–Ionic Ferroelectrics, Adv. Mater. 30 (2018) 1803716.
(18) J. Harada, N. Yoneyama, S. Yokokura, Y. Takahashi, A. Miura, N. Kitamura, T. Inabe, Ferroelectricity and Piezoelectricity in Free-Standing Polycrystalline Films of Plastic Crystals, J. Am. Chem. Soc. 140 (2018) 346–354.
(19) J. Harada, Y. Kawamura, Y. Takahashi, Y. Uemura, T. Hasegawa, H. Taniguchi, K. Maruyama, Plastic/Ferroelectric Crystals with Easily Switchable Polarization: Low-Voltage Operation, Unprecedentedly High Pyroelectric Performance, and Large Piezoelectric Effect in Polycrystalline Forms, J. Am. Chem. Soc. 141 (2019) 9349-9357.
(20) B. Wang, J. F. Hong, Y. T. Yang, H. X. Zhao, L. S. Long, L. S. Zheng, Achievement of a giant piezoelectric coefficient and piezoelectric voltage coefficient through plastic molecular-based ferroelectric materials, Matter 5 (2022) 1296-1304.
(21) M. P. Zheng, Y. D. Hou, M. K. Zhu, H. Yan, Research Progress of Piezoelectric Ceramics for Energy Harvesting, J. Chin. Ceram. Soc. 44 (2016) 359-366.

(22) X. Y. Gao, C. R. Qiu, G. Li, M. Ma, S. Yang, Z. Xu, F. Li, High output power density of a shear-mode piezoelectric energy harvester based on $Pb(In_{1/2}Nb_{1/2})O_3$-$Pb(Mg_{1/3}Nb_{2/3})O_3$-$PbTiO_3$ single crystals, Appl. Energ. 271 (2020) 115193.
(23) M. Y. Li, H. J. Wondergem, M. J. Spijkman, K. Asadi, I. Katsouras, P. W. M. Blom, D. M. de Leeuw, Revisiting the δ-phase of poly(vinylidene fluoride) for solution-processed ferroelectric thin films. Nat. Mater. 12 (2013) 433-438.
(24) S. Deswal, S. K. Singh, R. Pandey, P. Nasa, D. Kabra, B. Praveenkumar, S. Ogale, R. Boomishanka, Neutral 1D Perovskite-Type ABX3 Ferroelectrics with High Mechanical Energy Harvesting Performance, Chem. Mater. 32 (2020) 8333-8341.
(25) A. A. Khan, G. G. Huang, M. M. Rana, N. Q. Mei, M. Biondi, S. Rassel, N. Tanguy, B. Sun, Z. Leonenko, N. Yan, C. L. Wang, S. H. Xu, D. Y. Ban, Superior transverse piezoelectricity in organic-inorganic hybrid perovskite nanorods for mechanical energy harvesting, Nano Energy 86 (2021) 106039.
(26) S. Deswal, S. K. Singh, P. Rambabu, P. Kulkarni, G. Vaitheeswaran, B. Praveenkumar, S. Ogale, R. Boomishankar, Flexible Composite Energy Harvesters from Ferroelectric A_2MX_4-Type Hybrid Halogenometallates, Chem. Mater 31 (2019) 4545-4552.
(27) J. Dhar, S. Sil, N. A. Hoque, A. Dey, S. Das, P. P. Ray, D. Sanyal, Lattice-Defect-Induced Piezo Response in Methylammonium-Lead-Iodide Perovskite Based Nanogenerator, ChemistrySelect 3 (2018) 5304-5312.
(28) T. M. Guo, Y. J. Gong, Z. G. Li, Y. M. Liu, W. Li, Z. Y. Li, X. H. Bu, A New Hybrid Lead-Free Metal Halide Piezoelectric for Energy Harvesting and Human Motion Sensing, Small 18 (2022) 2103829.
(29) S. Ippili, V. Jella, J. Kim, S. Hong, S. G. Yoon, Unveiling Predominant Air-Stable Organotin Bromide Perovskite toward Mechanical Energy Harvesting, ACS Appl. Mater. Interfaces 12 (2020) 16469-16480.
(30) T. Vijayakanth, A. K. Srivastava, F. Ram, P. Kulkarni, K. Shanmuganathan, B. Praveenkumar, R. Boomishankar, A Flexible Composite Mechanical Energy Harvester from a Ferroelectric Organoamino Phosphonium Salt, Angew. Chem. Int. Ed. 57 (2018) 9054-9058.
(31) R. Ding, He. Liu, X. L. Zhang, J. X. Xiao, R. Kishor, H. X. Sun, B. W. Zhu, G. Chen, F. Gao, X. H. Feng, J. S. Chen, X. D. Chen, X. W. Sun, Y. J. Zheng, Flexible Piezoelectric Nanocomposite Generators Based on Formamidinium Lead Halide Perovskite Nanoparticles, Adv. Funct. Mater. 26 (2016) 7708-7716.